



OPEN

Atomically thin nonreciprocal optical isolation

Xiao Lin^{1,2,3}, Zuojia Wang^{1,2}, Fei Gao³, Baile Zhang^{3,4} & Hongsheng Chen^{1,2}

SUBJECT AREAS:

OPTICAL PROPERTIES AND
DEVICES

MAGNETO-OPTICS

Received

16 October 2013

Accepted

20 January 2014

Published

26 February 2014

Correspondence and
requests for materials
should be addressed to
H.S.C. (hansomchen@
zju.edu.cn) or B.L.Z.
(blzhang@ntu.edu.sg)

¹State Key Laboratory of Modern Optical Instrumentation, Zhejiang University, Hangzhou 310027, China, ²The Electromagnetics Academy at Zhejiang University, Zhejiang University, Hangzhou 310027, China, ³Division of Physics and Applied Physics, School of Physical and Mathematical Sciences, Nanyang Technological University, Singapore 637371, Singapore, ⁴Centre for Disruptive Photonic Technologies, Nanyang Technological University, Singapore 637371, Singapore.

Optical isolators will play a critical role in next-generation photonic circuits, but their on-chip integration requires miniaturization with suitable nonreciprocal photonic materials. Here, we theoretically demonstrate the thinnest possible and polarization-selective nonreciprocal isolation for circularly polarized waves by using graphene monolayer under an external magnetic field. The underlying mechanism is that graphene electron velocity can be largely different for the incident wave propagating in opposite directions at cyclotron frequency, making graphene highly conductive and reflective in one propagation direction while transparent in the opposite propagation direction under an external magnetic field. When some practical loss is introduced, nonreciprocal isolation with graphene monolayer still possesses good performance in a broad bandwidth. Our work shows the first study on the extreme limit of thickness for optical isolation and provides theoretical guidance in future practical applications.

Optical isolators, the photonic analogue of diodes, allow nonreciprocal unidirectional light transmission^{1–8}. They have become indispensable components in optical telecommunications and laser applications for stabilizing propagating photons and preventing undesired feedback^{1–8}. However, the main component of the optical isolators, Faraday rotator, is usually composed of magneto-optical materials with weak Faraday effect. It requires a long propagation distance in the order of operating wavelength to achieve good isolation, and therefore, optical isolators are generally bulky¹. In attempt to reduce costs and realize on-chip integration, there is a keen interest to miniaturize the nonreciprocal devices through designing novel structures². Recent advance in fabrication of ultrathin two-dimensional (2D) graphene down to monolayer may provide the possibility to further push the optical isolation to atomic scale and has attracted more and more people's interests. This is due to the fact that graphene can become nonreciprocal and gyrotropic under an external magnetic field^{9–16}. However, because of its ultrathin thickness, graphene is almost transparent for light^{17,18}, and can only turn the polarization of incident light by several degrees under a modest magnetic field^{11,12}. Hence, external bulky resonating structure and polarizer are still needed when incorporating graphene into the traditional isolators^{13,14}. Achieving optical isolation in the atomic scale is still very challenging.

In this paper, we theoretically proposed the idea of atomically thin nonreciprocal optical isolation for circularly polarized waves by using graphene monolayer. We show that under an external magnetic field, electrons in graphene would experience distinct magnitudes of Lorentz force for left-handed or right-handed circularly polarized wave (LCP or RCP) incidence at cyclotron frequency. Therefore, for the same circularly polarized wave, graphene can be tailored to be transparent to the forward propagation direction, whereas to be reflective to the backward propagation direction. Moreover, for the same propagation direction, graphene can be tailored to be transparent to one of the circularly polarized waves, whereas to be reflective to the other polarization handedness. As a result, the polarization-selective isolator can isolate and filter circular polarizations simultaneously. Our work provides an analytical study on the extreme limit of thickness for optical isolation, which might be useful in the quest to miniaturize nonreciprocal photonics in the future.

Results

Fig. 1 schematically shows the atomically thin and polarization-selective optical isolation based on graphene monolayer. Under an external magnetic field perpendicular to graphene plane, graphene (in the *xy* plane)

becomes gyrotropic and can be described by an asymmetric permittivity tensor: $\vec{\epsilon} = \begin{pmatrix} \epsilon & i\epsilon_g & 0 \\ -i\epsilon_g & \epsilon & 0 \\ 0 & 0 & \epsilon_z \end{pmatrix}$. For

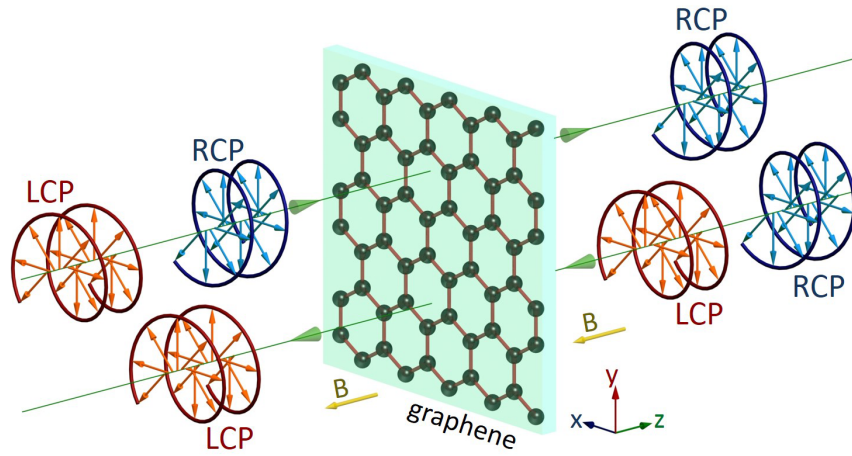


Figure 1 | Schematics of the atomically thin and polarization-selective optical isolation for circularly polarized waves. An external magnetic field is applied perpendicular to graphene plane. Only one circularly polarized wave can propagate through the gyrotropic graphene in one propagation direction. The arrows in the helices show the instantaneous electric field distributions of circularly polarized waves.

plane wave propagating along magnetization ($\pm \hat{z}$) direction, the eigenmodes in gyrotropic graphene are LCP and RCP. Without loss of generality, we analytically calculate the transmissivity of circularly polarized waves normally incident from a dielectric medium with relative permittivity ε_1 onto the gyrotropic graphene layer, and transmitted into a second dielectric medium with relative permittivity ε_3 . Detailed calculation can be found in *Methods*. The calculated wavevectors for LCP and RCP in gyrotropic graphene are as follows:

$$\begin{aligned} k^{+LCP} &= \omega/c\sqrt{\varepsilon + \varepsilon_g} \quad \& \\ k^{+RCP} &= \omega/c\sqrt{\varepsilon - \varepsilon_g} \quad \text{for forward propagation } (+\hat{z}), \\ k^{-LCP} &= \omega/c\sqrt{\varepsilon - \varepsilon_g} \quad \& \\ k^{-RCP} &= \omega/c\sqrt{\varepsilon + \varepsilon_g} \quad \text{for backward propagation } (-\hat{z}), \end{aligned} \quad (1)$$

from which we see that for the same circularly polarized wave they have different phase velocities ($v_{ph} = \omega/k$) in the forward and backward propagations. Moreover, since $|k^{+LCP}| = |k^{-RCP}|$ and $|k^{-LCP}| = |k^{+RCP}|$, the transmissivity of LCP in one propagation direction is the same with that of RCP in the opposite propagation direction. With this symmetry, we only need to analyze the forward propagating transmissivity.

The ideal case of graphene monolayer without loss is firstly discussed in Fig. 2(a). The parameters in Fig. 2(a) are as follows: the chemical potential $\mu_c = 0.5$ eV, the cyclotron frequency $\omega_c/2\pi = 10$ THz, the damping constant $\gamma = 0$, and $\varepsilon_1 = \varepsilon_3 = 1$. From the analytical derivations (details are in *Methods*), we can get forward propagating transmissivity $t^{+LCP} = 0$ and $t^{+RCP} = 0.99$ at cyclotron frequency, indicating good isolation performance. The underlying mechanism of the remarkable contrast in transmissivity at cyclotron frequency is that the electron velocity in graphene under LCP incidence is largely different from that under RCP incidence, making gyrotropic graphene highly conductive and reflective for one circular polarization incidence while transparent for another circular polarization incidence. From a microscopic point of view, by using free electron model¹⁹, $m_{eff} d\bar{v}/dt = -e(\bar{E} + \bar{v} \times \bar{B})$, where m_{eff} is the effective electron mass and \bar{E} is the electric field of incident wave being either RCP or LCP. Under time harmonic excitation, we can derive

$$\bar{v} = \frac{-e[i\omega\bar{E} + \bar{\omega}_c \times \bar{E} - \frac{i}{\omega}\bar{\omega}_c(\bar{\omega}_c \cdot \bar{E})]}{m_{eff}(\omega^2 - \omega_c^2)} \quad (2)$$

where $\bar{\omega}_c = -e\bar{B}/m_{eff}$. In this paper, we set the external magnetic field \bar{B} along $-\hat{z}$ direction, and the scalar cyclotron angular frequency

is defined as $\omega_c = |\bar{\omega}_c|$. For the forward ($+\hat{z}$) propagation, we have $\bar{v}^{+LCP} = \frac{-ie\bar{E}^{+LCP}}{m_{eff}(\omega - \omega_c)}$ for LCP incidence with $\bar{E}^{+LCP} = E_0(\hat{x} - i\hat{y})$ and $\bar{v}^{+RCP} = \frac{-ie\bar{E}^{+RCP}}{m_{eff}(\omega + \omega_c)}$ for RCP incidence with $\bar{E}^{+RCP} = E_0(\hat{x} + i\hat{y})$. Hence, the magnitude of Lorentz force acting on graphene electrons under LCP incidence ($|F^{+LCP}| = |\frac{-e\omega\bar{E}^{+LCP}}{(\omega - \omega_c)}|$) is much larger than that under RCP incidence ($|F^{+RCP}| = |\frac{-e\omega\bar{E}^{+RCP}}{(\omega + \omega_c)}|$) at $\omega = \omega_c$. As a result, $\bar{v}_{B \neq 0}^{+LCP}$ can be theoretically very large and $\bar{v}_{B \neq 0}^{+RCP}$ is reduced to half at cyclotron frequency. Since the electric current density $\bar{J} \propto \bar{v}$ and $\bar{J} = \sigma\bar{E}$, gyrotropic graphene becomes highly conductive under LCP incidence, indicating gyrotropic graphene behaves like a perfect electric conductor, and LCP is thus totally reflected. In

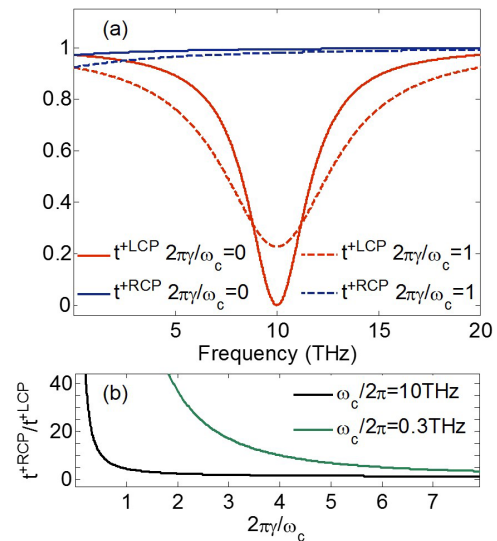


Figure 2 | Transmissivity of RCP (t^{+RCP}) and LCP (t^{+LCP}) through gyrotropic graphene monolayer in the forward propagation. (a) Comparison of t^{+RCP} and t^{+LCP} under the lossless ($2\pi\gamma/\omega_c = 0$) and loss ($2\pi\gamma/\omega_c = 1$) conditions with $\omega_c/2\pi = 10$ THz. (b) Loss influence on the isolation performance with different cyclotron frequencies. t^{+RCP}/t^{+LCP} increases as $2\pi\gamma/\omega_c$ or ω_c decreases. Other parameters are as follows: $\mu_c = 0.5$ eV and $\varepsilon_1 = \varepsilon_3 = 1$.



contrast, for RCP incidence, graphene has a finite negative permittivity and wave is evanescent inside of the graphene. As its skin depth ($1/\text{Im}(k^{+RCP}) > 100$ nm) is far larger than graphene's atomic thickness, graphene is highly transparent to RCP incident wave.

Because of the collision between electrons, loss is inevitable in practical graphene samples. In the following part, we studied the loss influence on the isolation performance. When loss is considered, the electron velocity in equation (2) becomes

$$\bar{v} = \frac{-e[i(\omega + i\gamma)\bar{E} + \bar{\omega}_c \times \bar{E} - \frac{i}{\omega} \bar{\omega}_c(\bar{\omega}_c \cdot \bar{E})]}{m_{\text{eff}}((\omega + i\gamma)^2 - \omega_c^2)}. \text{ For the forward (+}\hat{z}\text{)}$$

propagation and by setting \bar{B} along $-\hat{z}$ direction, we have

$$\bar{v}^{+LCP} = \frac{-ie\bar{E}^{+LCP}}{m_{\text{eff}}(\omega + i\gamma - \omega_c)} \text{ for LCP incidence and } \bar{v}^{+RCP} = \frac{-ie\bar{E}^{+RCP}}{m_{\text{eff}}(\omega + i\gamma + \omega_c)} \text{ for RCP incidence. Therefore, as long as } 2\pi\gamma/\omega_c$$

is sufficiently small, $\bar{v}_{B \neq 0}^{+LCP}$ can still be theoretically very large, and $\bar{v}_{B \neq 0}^{+LCP} \gg \bar{v}_{B \neq 0}^{+RCP}$ at cyclotron frequency can still be achieved. Fig. 2(a) shows the analytical transmissivity of LCP and RCP under the lossless ($2\pi\gamma/\omega_c = 0$) and loss ($2\pi\gamma/\omega_c = 1$) conditions. One can see that the loss degrades the performance of isolation. Fig. 2(b) shows the transmissivity ratio between RCP and LCP at cyclotron frequency (t^{+RCP}/t^{+LCP}) as a function of $2\pi\gamma/\omega_c$ with different cyclotron frequencies, from which one can see that, on one hand, t^{+RCP}/t^{+LCP} increases as $2\pi\gamma/\omega_c$ decreases, on the other hand, with the same value of $2\pi\gamma/\omega_c$, t^{+RCP}/t^{+LCP} increases as the cyclotron frequency decreases. Hence, better isolation performance can be obtained by keeping $2\pi\gamma/\omega_c$ sufficiently small or setting smaller cyclotron frequency.

To verify the analytical prediction of the atomically thin isolation, Fig. 3 shows the numerical simulations of the lossless case at 10 THz with the use of Finite Element Method (COMSOL Multiphysics). In the simulation, the following parameters are used: $\mu_c = 0.5$ eV, $\omega_c/2\pi = 10$ THz, $\gamma = 0$, and $\varepsilon_1 = \varepsilon_3 = 1$. We set the incident field with unit magnitude. When propagating in the forward direction, RCP is almost totally transmitted through graphene, as shown in Fig. 3(a), featured with unit magnitude of maximum E_y at both sides of graphene. Meanwhile, LCP is totally reflected, as shown in Fig. 3(b), characterized with twice unit magnitude of maximum E_y at the left graphene side and near zero at the right side. Moreover, from Fig. 3(b), one can see that the total electric field at the graphene boundary is always zero, indicating that graphene exhibits zero impedance, verifying our previous theoretical analysis that in this case graphene behaves like a highly conductive material. When propagating in the backward direction, RCP is totally reflected in Fig. 3(c) and LCP is almost totally transmitted in Fig. 3(d), behaving inversely to the forward propagation.

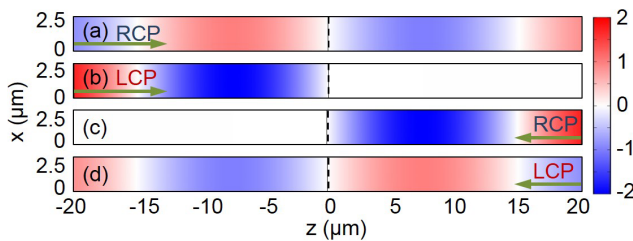


Figure 3 | Simulation demonstration of the atomically thin optical isolation for circularly polarized waves under the lossless condition. E_y field distribution of RCP and LCP waves propagating in (a–b) the forward (+ \hat{z}) and (c–d) backward ($-\hat{z}$) directions at 10 THz. The black dashed lines denote the location of graphene and the green arrows represent the wave incident direction. The parameters are: $\mu_c = 0.5$ eV, $\omega_c/2\pi = 10$ THz, $\gamma = 0$, and $\varepsilon_1 = \varepsilon_3 = 1$. Under the lossless condition, graphene monolayer can isolate and filter the circular polarizations simultaneously.

The numerical verifications for the loss case are shown in Fig. 4. Based on previous practical graphene parameters, we set $\omega_c/2\pi = 0.3$ THz, $\mu_c = 0.5$ eV, and $\gamma = 0.63$ THz in the demonstration. These correspond to $B = -1$ Tesla, the 2D carrier density $n_s = 2 \times 10^{13}$ cm $^{-2}$, and the electron mobility $\mu = 28000$ cm 2 V $^{-1}$ s $^{-1}$. These parameter settings are achievable in experiments, because that the 2D carrier density n_s in graphene is experimentally reported to be gated efficiently from very low (10^{10} cm $^{-2}$) to very high values (10^{14} cm $^{-2}$)^{20–22}, and the electron mobility up to $\mu = 60000$ cm 2 V $^{-1}$ s $^{-1}$ has been experimentally obtained in high-quality suspended²³ or hexagonal boron nitride substrate supported²⁴ graphene samples. We also consider the graphene is mounted on a substrate. The influence of surrounding dielectric substrate on the isolating performance is shown in Fig. 4(a,b), where symmetric structure is assumed with $\varepsilon_1 = \varepsilon_3 = \varepsilon_d$ to avoid additional back-ground reflection. Smaller ε_d is found favorable to achieve better isolation performance. To ensure the high electron mobility in graphene and therefore a smaller damping constant γ , hexagonal boron nitride with $\varepsilon_d = 4.8$ ²⁵ is chosen. From Fig. 4(b), one can see that high t^{+RCP}/t^{+LCP} can be obtained in a wide frequency range with the maxima of 25.96 at 0.311 THz (3.7% higher than $\omega_c = 0.3$ THz). When $t^{+RCP}/t^{+LCP} > 10$ is defined as a reference, a 0.26 THz bandwidth can be obtained with frequency ranging from 0.2 to 0.46 THz. Fig. 4(c–f) show the numerical simulations of the nonreciprocal isolation at 0.3 THz. In the forward propagation, RCP wave passes graphene with a transmissivity of 31.5% in Fig. 4(c), while LCP is efficiently blocked with a trivial transmissivity of 1.23% in Fig. 4(d). When propagating in the backward direction, it behaves inversely in Fig. 4(e,f). From these demonstration, one see that an atomically thin wide-band THz nonreciprocal optical isolation is possible by using practical graphene samples, showing the appealing potential applications of graphene in ultrathin nonreciprocal device design.

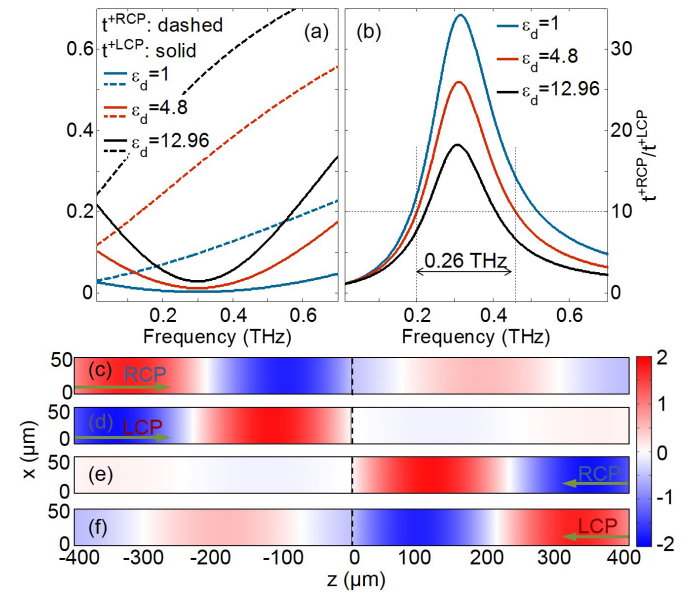


Figure 4 | Atomically thin optical isolation under the loss condition. (a) Influence of ε_d on the forward propagating transmissivity of LCP and RCP waves, where $\varepsilon_1 = \varepsilon_3 = \varepsilon_d$. (b) The isolation performance represented by t^{+RCP}/t^{+LCP} for different ε_d . (c–f) E_y field distribution of circularly polarized waves propagating in the forward (+ \hat{z}) and backward ($-\hat{z}$) directions at 0.3 THz. The Parameters are: $\mu_c = 0.5$ eV, $\omega_c/2\pi = 0.3$ THz, $\gamma = 0.63$ THz, and $\varepsilon_d = 4.8$. The black dashed lines denote the location of graphene, and the green arrows represent the wave incident direction.



Discussion

Previous graphene based traditional Faraday isolators^{14,16} are generally composed by a graphene sheet, a resonating structure and two wire grids. In that Faraday isolator structure, the gyrotropic graphene only serves as a Faraday rotator, the thickness of the resonating structure is around half of the operating wavelength¹⁴, and the two wire grids serving as the polarizers are indispensable to realize isolation. When considering the thickness of the resonating structure and wire grids, the total thickness of previous graphene based Faraday isolators^{14,16} is usually in the order of operating wavelength, far larger than our atomic thickness. Hence, previous graphene based Faraday isolators^{14,16} are different from the demonstration in this work where no external wire grids or other resonant structures are needed. Flexible tunability is a potential advantage of graphene based devices^{26,27}. Since the best performance of the ultrathin graphene isolation exists near cyclotron frequency, the isolation working frequency range should also be tunable by external magnetic field.

In conclusion, we have theoretically proposed the atomically thin and polarization-selective nonreciprocal optical isolation for circular polarizations. The mechanism underlying the atomically thin optical isolator is revealed from a microscopic viewpoint. Our work shows a feasible solution to control the propagation of circularly polarized waves in graphene and to manipulate light nonreciprocally at atomic scale, which opens up new possibilities for further innovations in functional ultrathin nonreciprocal optics.

Methods

Graphene monolayer is treated as a homogeneous film with thickness $d = 1 \text{ nm}$ ^{20,28} and characterized by an anisotropic permittivity tensor $\text{diag}[\epsilon_{eq} \epsilon_{eq} \epsilon_z]$. Based on Kubo formula, ϵ_{eq} can be cast to the Drude model^{9,10,20,28,29},

$$\epsilon_{eq} = 1 + i \frac{G_{\text{intra}} + G_{\text{inter}}}{\omega \epsilon_0 d} = \epsilon_{\text{inter}} + i \frac{G_{\text{intra}}}{\omega \epsilon_0 d} = \epsilon_{\text{inter}} - \frac{\omega_p^2}{\omega(\omega + i\gamma)} \quad (3)$$

where $G_{\text{intra}} = \frac{ie^2 k_B T}{\pi \hbar^2 (\omega + i\gamma)} \left(\frac{\mu_c}{k_B T} + 2 \ln(e^{-\mu_c/k_B T} + 1) \right)$ and G_{inter} are optical conductivity attributed to intra-band and inter-band transitions respectively, $\epsilon_{\text{inter}} = 1 + i G_{\text{inter}} / \omega \epsilon_0 d$, $\omega_p = \left[\frac{e^2 k_B T}{\pi \hbar^2 \epsilon_0 d} \left(\frac{\mu_c}{k_B T} + 2 \ln(e^{-\mu_c/k_B T} + 1) \right) \right]^{1/2}$ is the plasma frequency, γ is the inverse of relaxation time, and ϵ_0 , e , \hbar , and k_B are the dielectric permittivity in vacuum, electron charge, reduced Planck constant, and Boltzmann constant, respectively. When setting $\mu_c = 0.5 \text{ eV}$ and temperature $T = 300 \text{ K}$, we have the effective electron mass $m_{\text{eff}} = 0.1 \times 0.91 \times 10^{-30} \text{ kg}$ and $\omega_p / 2\pi = 410 \text{ THz}$. At the operation frequency below 1 THz , ϵ_{inter} is equal to 3.9.

Gyrotropic graphene can be described by an asymmetric permittivity tensor

$$\bar{\epsilon} = \begin{pmatrix} \epsilon & i\epsilon_g & 0 \\ -i\epsilon_g & \epsilon & 0 \\ 0 & 0 & \epsilon_z \end{pmatrix}, \text{ where } \epsilon = \epsilon_{\text{inter}} - \omega_p^2 / (\omega(\omega + i\gamma)) / [\omega((\omega + i\gamma)^2 - \omega_c^2)] \text{ and}$$

$\epsilon_g = -\omega_p^2 \omega_c / [\omega((\omega + i\gamma)^2 - \omega_c^2)]$. Hence, $\epsilon + \epsilon_g = \epsilon_{\text{inter}} - \omega_p^2 / (\omega(\omega - \omega_c + i\gamma))$ and $\epsilon - \epsilon_g = \epsilon_{\text{inter}} - \omega_p^2 / (\omega(\omega + \omega_c + i\gamma))$. The scalar cyclotron angular frequency ω_c is defined as $|\bar{\omega}_c|$, when the external magnetic field \bar{B} is along $-\hat{z}$ direction.

Wave polarizations can be viewed by either the temporal or spatial view points. In the case of a circularly polarized wave, from the temporal view point, the tip of the electric field vector describes a circle at a fixed point in space as time progresses. If the right-hand (left-hand) thumb points in the direction of propagation while the fingers point in the direction of the tip motion, the wave is defined as right-hand (left-hand) circularly polarized. From the spatial view point, the instantaneous electric field vector of the RCP (LCP) wave describes a left-hand (right-hand) helix along the direction of propagation, as shown in Fig. 1.

To achieve the condition of good isolation for circular polarizations, the transmissivity of the forward propagation in Fig. 1 are analytically calculated in the following. The calculation of backward propagation can be done by the same methodology. Setting $\bar{E}_l^{L/RCP} = (A_l^{L/RCP} e^{ik_l^{L/RCP} z} + C_l^{L/RCP} e^{-ik_l^{L/RCP} z}) (\hat{x} \mp i\hat{y})$ in the l^{th} region with $l = 2$ standing for gyrotropic graphene and $l = 1, 3$ for isotropic dielectric. After calculation, we have:

$$\frac{C_l^{L/RCP}}{A_l^{L/RCP}} = \frac{R_{l(l+1)}^{L/RCP} e^{i2k_{l+1}^{L/RCP} d} + (C_{l+1}^{L/RCP} / A_{l+1}^{L/RCP}) e^{i2k_l^{L/RCP} d}}{e^{i2k_{l+1}^{L/RCP} d} + R_{l(l+1)}^{L/RCP} (C_{l+1}^{L/RCP} / A_{l+1}^{L/RCP})} \quad (4)$$

$$\text{where } R_{l(l+1)}^{L/RCP} = \frac{1 - P_{l(l+1)}^{L/RCP}}{1 + P_{l(l+1)}^{L/RCP}}, T_{l(l+1)}^{L/RCP} = \frac{2}{1 + P_{l(l+1)}^{L/RCP}}, P_{12}^{L/RCP} = \frac{k_1(\epsilon \pm \epsilon_g)}{k_2^{L/RCP} \epsilon_1},$$

$P_{23}^{L/RCP} = \frac{k_2^{L/RCP} \epsilon_3}{k_3(\epsilon \pm \epsilon_g)}$, $k_{1,3}^{L/RCP} = \omega / c \sqrt{\epsilon_{1,3}}$, $k_2^{L/RCP} = \omega / c \sqrt{\epsilon \pm \epsilon_g}$, $C_3^{L/RCP} = 0$, $d_{z1} = 0$, and $d_{z2} = d$. The reflection and transmission coefficients are $R^{L/RCP} = C_1^{L/RCP} / A_1^{L/RCP}$ and $T^{L/RCP} = A_3^{L/RCP} / A_1^{L/RCP}$, respectively. After some algebra, we have

$$R^{L/RCP} = \frac{R_{12}^{L/RCP} + R_{23}^{L/RCP} e^{i2k_2^{L/RCP} d}}{1 + R_{12}^{L/RCP} R_{23}^{L/RCP} e^{i2k_2^{L/RCP} d}} \\ = \frac{\sqrt{\epsilon_1} - \sqrt{\epsilon_{\text{inter}} - \frac{\omega_p^2}{\omega(\omega \mp \omega_c + i\gamma)}}}{\sqrt{\epsilon_1} + \sqrt{\epsilon_{\text{inter}} - \frac{\omega_p^2}{\omega(\omega \mp \omega_c + i\gamma)}}} + \frac{\sqrt{\epsilon_{\text{inter}} - \frac{\omega_p^2}{\omega(\omega \mp \omega_c + i\gamma)}} - \sqrt{\epsilon_3}}{\sqrt{\epsilon_{\text{inter}} - \frac{\omega_p^2}{\omega(\omega \mp \omega_c + i\gamma)}} + \sqrt{\epsilon_3}} e^{i2k_2^{L/RCP} d} \quad (5)$$

$$T^{L/RCP} = \frac{T_{12}^{L/RCP} T_{23}^{L/RCP} e^{i(k_2^{L/RCP} - k_3)d}}{1 + R_{12}^{L/RCP} R_{23}^{L/RCP} e^{i2k_2^{L/RCP} d}} \\ = \frac{2\sqrt{\epsilon_1}}{\sqrt{\epsilon_1} + \sqrt{\epsilon_{\text{inter}} - \frac{\omega_p^2}{\omega(\omega \mp \omega_c + i\gamma)}}} \frac{2\sqrt{\epsilon_3}}{\sqrt{\epsilon_{\text{inter}} - \frac{\omega_p^2}{\omega(\omega \mp \omega_c + i\gamma)}} + \sqrt{\epsilon_3}} e^{i(k_2^{L/RCP} - k_3)d} \\ = \frac{\sqrt{\epsilon_1} - \sqrt{\epsilon_{\text{inter}} - \frac{\omega_p^2}{\omega(\omega \mp \omega_c + i\gamma)}}}{\sqrt{\epsilon_1} + \sqrt{\epsilon_{\text{inter}} - \frac{\omega_p^2}{\omega(\omega \mp \omega_c + i\gamma)}}} \frac{\sqrt{\epsilon_{\text{inter}} - \frac{\omega_p^2}{\omega(\omega \mp \omega_c + i\gamma)}} - \sqrt{\epsilon_3}}{\sqrt{\epsilon_{\text{inter}} - \frac{\omega_p^2}{\omega(\omega \mp \omega_c + i\gamma)}} + \sqrt{\epsilon_3}} e^{i2k_2^{L/RCP} d} \quad (6)$$

The reflectivity and transmissivity are $r^{L/RCP} = |R^{L/RCP}|^2$ and

$t^{L/RCP} = |T^{L/RCP}|^2 \sqrt{\epsilon_3 / \epsilon_1}$, respectively. From equation (5) and equation (6), $r^{L/RCP}$ and $t^{L/RCP}$ are strongly dependent on ω_c , ω_p , and γ , when the operating frequency is around ω_c . In particular, for LCP incidence in the lossless case, when $\omega \rightarrow \omega_c$, $|\epsilon + \epsilon_g| = |\epsilon_{\text{inter}} - \omega_p^2 / (\omega(\omega - \omega_c))| \rightarrow \infty$, $|P_{12}^{LCP}| \rightarrow \infty$, $|P_{23}^{LCP}| = 0$, $R_{12}^{LCP} = -1$, $R_{23}^{LCP} = 1$, $T_{12}^{LCP} = 0$, $T_{23}^{LCP} = 2$, and thus $r^{LCP} = 1$ and $t^{LCP} = 0$. For RCP incidence in the lossless case at $\omega = \omega_c$, $\epsilon - \epsilon_g = \epsilon_{\text{inter}} - \omega_p^2 / (\omega(\omega + \omega_c))$ is negatively large but finite, and we get $t^{LCP} = 0.99$ as shown in Fig. 2(a) through numerical computation. When considering the loss case and setting ω_p as a constant, $t^{L/RCP}$ is strongly dependent on $2\pi\gamma/\omega_c$ and ω_c , which can be seen from Fig. 2(b).

When μ_c and γ are given, the corresponding n_s and μ can be theoretically calculated by using $n_s = \mu_c^2 / (\pi \hbar^2 v_F^2)^{10,29}$ and $1/\gamma = \mu_c \mu / (e v_F^2)^{10,29}$, respectively, where Fermi velocity $v_F \approx 0.95 \times 10^6 \text{ m/s}$. When $|B| = 1 \text{ Tesla}$ and $\mu_c = 0.5 \text{ eV}$, we can neglect Landau quantization influence and use the Drude model directly for graphene according to Ref. [10], because the following conditions are satisfied: the Landau energy scale $L = (2\hbar e B v_F^2)^{1/2} = 0.035 \text{ eV} \ll \mu_c$ and the operating frequency (set below 1 THz) energy $\hbar\omega \ll \mu_c$.

- Liu, M. & Zhang, X. Plasmon-boosted magneto-optics. *Nat. Photonics* **7**, 429–430 (2013).
- Chin, J. Y. *et al.* Nonreciprocal plasmonics enables giant enhancement of thin-film Faraday rotation. *Nat. Commun.* **4**, 1599 (2013).
- Khanikaev, A. B., Mousavi, S. H., Shvets, G. & Kivshar, Y. S. One-way extraordinary optical transmission and nonreciprocal spoof plasmons. *Phys. Rev. Lett.* **105**, 126804 (2010).
- Yu, Z., Wang, Z. & Fan, S. One-way total reflection with one-dimensional magneto-optical photonic crystals. *Appl. Phys. Lett.* **90**, 121133 (2007).
- Tocci, M. D., Bloemer, M. J., Scalora, M., Dowling, J. P. & Bowden, C. M. Thin-film nonlinear optical diode. *Appl. Phys. Lett.* **66**, 23246 (1995).
- Shadrivov, I. V., Fedotov, V. A., Powell, D. A., Kivshar, Y. S. & Zheludev, N. I. Electromagnetic wave analogue of an electronic diode. *New J. Phys.* **13**, 033025 (2011).
- Fang, K., Yu, Z., Liu, V. & Fan, S. Ultracompact non-reciprocal optical isolator based on guided resonance in a magneto-optical photonic crystal slab. *Opt. Lett.* **36**, 4254–4256 (2011).
- Davoyan, A. R., Mahmoud, A. M. & Engheta, N. Optical isolation with epsilon-near-zero metamaterials. *Opt. Express* **21**, 3279–3286 (2013).
- Gusynin, V. P., Sharapov, S. G. & Carbotte, J. P. Magneto-optical conductivity in graphene. *J. Phys.: Condens. Matter* **19**, 026222 (2007).
- Sounas, D. L. & Caloz, C. Gyrotropy and nonreciprocity of graphene for microwave applications. *IEEE Trans. Microw. Theory Tech.* **60**, 901–914 (2012).



11. Crassee, I. *et al.* Giant Faraday rotation in single- and multilayer graphene. *Nat. Phys.* **7**, 48–51 (2011).
12. Crassee, I. *et al.* Intrinsic terahertz plasmons and magnetoplasmons in large scale monolayer graphene. *Nano Lett.* **12**, 2470–2474 (2012).
13. Zhou, Y. *et al.* Tunable magnetoplasmons for efficient terahertz modulator and isolator by gated monolayer graphene. *Phys. Chem. Chem. Phys.* **15**, 5084–5090 (2013).
14. Sounas, D. L. & Caloz, C. Graphene-based non-reciprocal spatial isolator. Paper presented at *Proc. IEEE International Symposium on Antennas and Propagation (APSURSI)* 1597–1600, Spokane, WA, USA. DOI: 10.1109/APS.2011.5996606 (2011, July 3–8). Available at: <http://ieeexplore.ieee.org/xpl/login.jsp?tp=&arnumber=5996606&url=http%3A%2F%2Fieeexplore.ieee.org%2Fiel5%2F5981577%2F5996365%2F05996606.pdf%3Farnumber%3D5996606> (Accessed: 2014, Jan. 17).
15. Sounas, D. L. & Caloz, C. Electromagnetic nonreciprocity and gyrotropy of graphene. *Appl. Phys. Lett.* **98**, 021911 (2011).
16. Sounas, D. L. & Caloz, C. Gyrotropic properties of graphene and subsequent microwave applications. Paper presented at *Proc. 41st European Microwave Conference (EuMc)* 1142–1145 Manchester (2011, Oct. 10–13). Available at: http://ieeexplore.ieee.org/xpl/articleDetails.jsp?tp=&arnumber=6102014&url=http%3A%2F%2Fieeexplore.ieee.org%2Fxppls%2Fabs_all.jsp%3Farnumber%3D6102014 (Accessed: 2014, Jan. 17).
17. Nair, R. R. *et al.* Fine structure constant defines visual transparency of graphene. *Science* **320**, 1308 (2008).
18. Lin, X. *et al.* Ab initio study of electronic and optical behavior of two-dimensional silicon carbide. *J. Mater. Chem. C* **1**, 2131–2135 (2013).
19. Kong, J. A. *Electromagnetic Wave Theory* (EMW Publishing Cambridge Massachusetts USA, 2008).
20. Ju, L. *et al.* Graphene plasmonics for tunable terahertz Metamaterials. *Nat. Nanotech.* **6**, 630–634 (2011).
21. Das, A. *et al.* Monitoring dopants by Raman scattering in an electrochemically top-gated graphene transistor. *Nat. Nanotech.* **3**, 210–215 (2008).
22. Efetov, D. K. & Kim, P. Controlling electron-phonon interactions in graphene at ultrahigh carrier densities. *Phys. Rev. Lett.* **105**, 256805 (2010).
23. Bolotin, K. I. *et al.* Ultrahigh electron mobility in suspended graphene. *Solid State Commun.* **146**, 351–355 (2008).
24. Dean, C. R. *et al.* Boron nitride substrates for high-quality graphene electronics. *Nat. Nanotech.* **5**, 722–726 (2010).
25. Lin, X. *et al.* Ab initio optical study of graphene on hexagonal boron nitride and fluorographene substrates. *J. Mater. Chem. C* **1**, 1618–1627 (2013).
26. Fang, Z. *et al.* Gated Tunability and hybridization of localized plasmons in nanostructured graphene. *ACS nano* **7**, 2388–2395 (2013).
27. Fang, Z. *et al.* Active tunable absorption enhancement with graphene nanodisk arrays. *Nano Lett.* **14**, 299–304 (2014).
28. Vakil, A. & Engheta, N. Transformation optics using graphene. *Science* **332**, 1291–1294 (2011).
29. Hanson, G. W. Dyadic Green's functions and guided surface waves for a surface conductivity model of graphene. *J. Appl. Phys.* **103**, 064302 (2008).

Acknowledgments

This work was sponsored by the National Natural Science Foundation of China under Grants No. 61322501, No. 61275183, and No. 60990322, the National Youth Top-notch Talent Support Program, the Foundation for the Author of National Excellent Doctoral Dissertation of PR China under Grant No. 200950, the Fundamental Research Funds for the Central Universities under Grant No. 2011QNA5020, the Chinese Scholarship Council Foundation under Grant No. 2011833070, the Program for New Century Excellent Talents (NCET-12-0489) in University, the K. P. Chao's High Technology Development Foundation, the Nanyang Technological University, and the Singapore Ministry of Education under Tier 1 Ref. No. RG 27/12 and Grant No. MOE2011-T3-1-005.

Author contributions

X.L., B.Z. and H.C. conceived the idea of the study. X.L. performed the analysis and numerical simulations. Z.W. and F.G. contributed in the calculation and interpretation. H.C. and B.Z. supervised the project. All of the authors interpreted the results. X.L., B.Z. and H.C. wrote the manuscript with input from others.

Additional information

Competing financial interests: The authors declare no competing financial interests.

How to cite this article: Lin, X., Wang, Z.J., Gao, F., Zhang, B.L. & Chen, H.S. Atomically thin nonreciprocal optical isolation. *Sci. Rep.* **4**, 4190; DOI:10.1038/srep04190 (2014).



This work is licensed under a Creative Commons Attribution-NonCommercial-NoDerivs 3.0 Unported license. To view a copy of this license, visit <http://creativecommons.org/licenses/by-nc-nd/3.0>